Integral Equation Solution to the Skin Effect Problem in Conductor Strips of Finite Thickness

Jean-Fu Kiang, *Member, IEEE*

Abstract—**The skin effect of single and coupled conductor strips of finite thickness is analyzed using the dyadic Green's function and the integral equation formulation. Galerkin's method is used to solve the integral equation for the dispersion characteristics. The effects of the geometrical and electrical parameters on the conductor loss are investigated. Results are compared with the literature and shown to be in good agreement. This approach is very useful for analyzing the electrical properties of interconnects in high-performance computer circuitries.**

I. Introduction

To calculate the conductor loss of microstrip lines, a perturbation method has usually been used. The surface currents for the lossless case are obtained first by either a quasi-TEM approximation [1]–[3] or a full-wave approach [4]. Then, the conductor loss is evaluated by using the surface resistance and the surface current. By using the surface resistance approximation, it is assumed that the strip thickness is much larger than the skin depth.

In [5], the equivalent surface impedance is used in the boundary condition from which an integral equation is derived. The conductor loss is then obtained by solving this integral equation. As in [4], it is assumed that the thickness of the strip is at least several skin depths, and is much smaller than the width of the strip. In [6], a complex resistive boundary condition is applied to solve for the propagation constant of thin superconducting striplines. It is assumed that the strip is thin compared with the superconducting penetration depth.

In [7] and [8], a skin loss expression is derived based on the incremental inductance rule, which was first proposed by Wheeler [9]. In this technique, the thickness of the conductors exposed to the electric field should be greater than several skin depths.

Finite element methods [3], [10]–[12] have been used to calculate the conductor loss. These approaches are based on either an electrostatic scalar potential [3] or a magnetic vector potential [10]–[12]. In the magnetic vector potential approach, only the longitudinal current component is considered. In [10], the ac resistance is derived from the power loss calculated from the current distribution in the cross section.

Manuscript received April 9, 1990; revised October 4, 1990.

The author was with the IBM Research Division, Thomas J. Watson Research Center, P.O. Box 218, Yorktown Heights, NY 10598. He is now with Bell Communications Research, 331 Newman Springs Road, Red Bank, NJ 07701-7020.

IEEE Log Number 9041946.

In [11], the thickness of the strip is assumed to be much smaller than the skin depth, and only surface current is considered.

In [13], a finite element method is used to calculate the attenuation constant of a copper microstrip at 77 K. The results are compared with the closed-form solution obtained by neglecting the effect of fringing fields [14]. In [15], a phenomenological equivalence method is proposed for characterizing a planar quasi-TEM transmission line with a thin normal conductor or superconductor strip. This method is based on various empirical formulas valid under different conditions.

In [16], a perturbation series and coupled integral equation approach is used to calculate the frequency-dependent resistance and inductance for quasi-TEM transmission lines with conductor strip of arbitrary cross section. A diffusion equation and a Laplace's equation are solved interior and exterior to the conductor, respectively. Then, the boundary condition is imposed on the interface to obtain a coupled integral equation from which the frequency-dependent resistance can be obtained.

In [17], the ac resistance of cylindrical conductors is calculated by first assuming an axially independent TM mode excitation. Then the field expressions in the regions exterior and interior to the conductors are derived in terms of equivalent electric and magnetic surface currents. The continuity of tangential fields on the conductor surfaces are imposed to obtain the frequency-dependent resistance.

The skin effect becomes important in high-performance computer circuitries [18], [19] and superconductor transmission lines [13]–[15], [20]. In [14], the surface impedance for both the normal-state and the superconducting striplines are derived. It is assumed that the width of the stripline is much larger than the dielectric thickness so that the fringing field can be neglected. In [20], an approximate solution of propagation and attenuation constants for superconductor interconnects is presented. However, only the TM mode is considered, and the effects of interconnect cross section and the fringing field are not taken into account.

In this paper, an integral equation formulation using the dyadic Green's function [21]–[23] is derived to solve for the dispersion relation of single and coupled conductor strips with finite thickness. In Section II, the integral equation formulation for a finite number of conductor strips is derived. In Section III, the Galerkin's method is used to obtain the matrix eigenvalue equations. Numerical results and discussions are presented in Section IV.

0018-9480/91/0300-0452$01.00 ©1991 IEEE

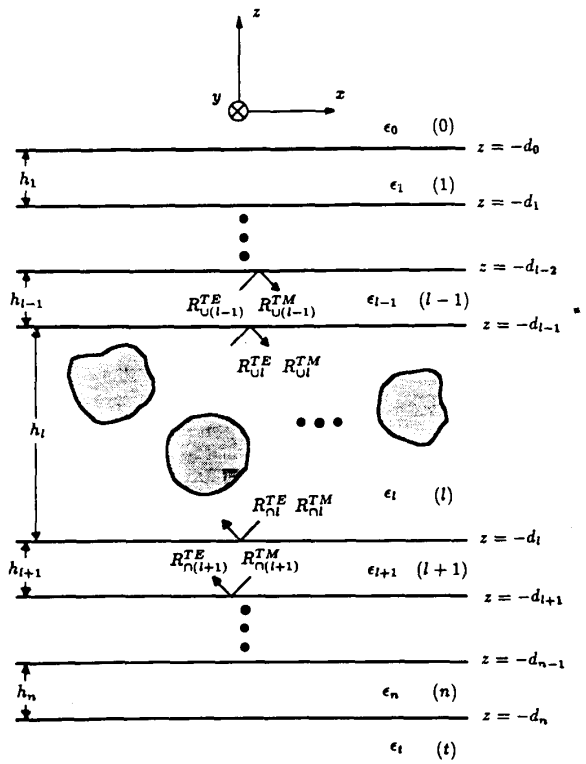

Fig. 1. Geometrical configuration of N conductor strips embedded in a multilayered medium.

II. Integral Equation Formulation

In Fig. 1, there are N conductor strips of arbitrary cross section embedded in layer (l) of a planar stratified medium. The whole structure is assumed to be uniform along the propagation direction y. Then, the electric field in layer (l) can be represented by the dyadic Green's function and the equivalent conduction and polarization current in the conductor strips as

$$\boldsymbol{E}(\boldsymbol{r}) = i\omega\mu_0 \iiint_V dV' \bar{\bar{G}}_{ll}(\boldsymbol{r},\boldsymbol{r}') \cdot \boldsymbol{J}_{eq}(\boldsymbol{r}')$$

$$= i\omega\mu_0 \iiint_V dV' \bar{\bar{G}}_{ll}(\boldsymbol{r},\boldsymbol{r}') \cdot \Delta\sigma(\boldsymbol{r}')\boldsymbol{E}(\boldsymbol{r}') \qquad (1)$$

where $\boldsymbol{J}_{eq}(\boldsymbol{r}) = \Delta\sigma(\boldsymbol{r})\boldsymbol{E}(\boldsymbol{r})$ with $\Delta\sigma(\boldsymbol{r}) = \sigma(\boldsymbol{r}) - \sigma_l - i\omega(\epsilon(\boldsymbol{r}) - \epsilon_l)$. The quantities $\epsilon(\boldsymbol{r})$ and $\sigma(\boldsymbol{r})$ are the permittivity and conductivity, respectively, in the cross section of the conductor strip; ϵ_l and σ_l are the background permittivity and conductivity, respectively, in layer (l); and V is the space occupied by the conductor strips. The dyadic Green's function $\bar{\bar{G}}_{ll}(\boldsymbol{r},\boldsymbol{r}')$ can be represented in the spectral domain as [22]

$$\bar{\bar{G}}_{ll}(\boldsymbol{r},\boldsymbol{r}') = \frac{i}{8\pi^2} \iint_{-\infty}^{\infty} d\boldsymbol{k}_s e^{i\boldsymbol{k}_s\cdot(\boldsymbol{r}_s - \boldsymbol{r}_s')} \bar{\bar{g}}_{ll}(\boldsymbol{k}_s, z, z') - \frac{\hat{z}\hat{z}}{k_l^2}\delta(\boldsymbol{r} - \boldsymbol{r}') \qquad (2)$$

where

$$\boldsymbol{k}_s = \hat{x}k_x + \hat{y}k_y$$

$$\boldsymbol{r}_s = \hat{x}x + \hat{y}y$$

$$\boldsymbol{r}_s' = \hat{x}x' + \hat{y}y'.$$

Here, the time-harmonic convention of $e^{-i\omega t}$ is used. The first term on the right-hand side of (2) is the principal value part of the dyadic Green's function, and the second term is the source dyadic. The source dyadic term shown in this spectral-domain solution is equivalent to using a thin disk as the exclusion volume in a principal value integration over a current region in the space domain. $\bar{\bar{g}}_{ll}(\boldsymbol{k}_s, z, z')$ is the Fourier transform of the principal value part of $\bar{\bar{G}}_{ll}(\boldsymbol{r},\boldsymbol{r}')$ with respect to $\boldsymbol{r}_s$.

For $z > z'$, the explicit form of $\bar{\bar{g}}_{ll}(\boldsymbol{k}_s, z, z')$ is given by [21]–[23]

$$\bar{\bar{g}}_{ll}(\boldsymbol{k}_s, z_>, z'_<) = \frac{1}{k_{lz}\left(1 - R^{TE}_{Ul}R^{TE}_{nl}e^{2ik_{lz}h_l}\right)} \cdot \left[\hat{h}(k_{lz})e^{ik_{lz}z_l} + R^{TE}_{Ul}\hat{h}(-k_{lz})e^{ik_{lz}(2h_l - z_l)}\right] \cdot \left[\hat{h}(k_{lz})e^{-ik_{lz}z_l'} + R^{TE}_{nl}\hat{h}(-k_{lz})e^{ik_{lz}z_l'}\right] + \frac{1}{k_{lz}\left(1 - R^{TM}_{Ul}R^{TM}_{nl}e^{2ik_{lz}h_l}\right)} \cdot \left[\hat{v}(k_{lz})e^{ik_{lz}z_l} + R^{TM}_{Ul}\hat{v}(-k_{lz})e^{ik_{lz}(2h_l - z_l)}\right] \cdot \left[\hat{v}(k_{lz})e^{-ik_{lz}z_l'} + R^{TM}_{nl}\hat{v}(-k_{lz})e^{ik_{lz}z_l'}\right] \qquad (3a)$$

and for $z < z'$, we have

$$\bar{\bar{g}}_{ll}(\boldsymbol{k}_s, z_<, z'_>) = \frac{1}{k_{lz}\left(1 - R^{TE}_{Ul}R^{TE}_{nl}e^{2ik_{lz}h_l}\right)} \cdot \left[\hat{h}(-k_{lz})e^{-ik_{lz}z_l} + R^{TE}_{nl}\hat{h}(k_{lz})e^{ik_{lz}z_l}\right] \cdot \left[\hat{h}(-k_{lz})e^{ik_{lz}z_l'} + R^{TE}_{Ul}\hat{h}(k_{lz})e^{ik_{lz}(2h_l - z_l')}\right] + \frac{1}{k_{lz}\left(1 - R^{TM}_{Ul}R^{TM}_{nl}e^{2ik_{lz}h_l}\right)} \cdot \left[\hat{v}(-k_{lz})e^{-ik_{lz}z_l} + R^{TM}_{nl}\hat{v}(k_{lz})e^{ik_{lz}z_l}\right] \cdot \left[\hat{v}(-k_{lz})e^{ik_{lz}z_l'} + R^{TM}_{Ul}\hat{v}(k_{lz})e^{ik_{lz}(2h_l - z_l')}\right] \qquad (3b)$$

where z_l and z_l' are the local coordinates defined as $z_l = z + d_l$, $z_l' = z' + d_l$, and

$$\hat{h}(\pm k_{lz}) = \frac{\hat{x}k_y - \hat{y}k_x}{k_s}$$

$$\hat{v}(\pm k_{lz}) = \mp\frac{k_{lz}\boldsymbol{k}_s}{k_l k_s} + \hat{z}\frac{k_s}{k_l} \qquad (4)$$

where $k_s = |\boldsymbol{k}_s|$, $k_{lz} = \sqrt{k_l^2 - k_s^2}$ with $\mathrm{Im}(k_{lz}) \geq 0$.

In (3), $R^{TM}_{\cup l}$ and $R^{TE}_{\cup l}$ are the reflection coefficients of the TM and the TE modes at the upper boundary of layer (l), and $R^{TM}_{\cap l}$ and $R^{TE}_{\cap l}$ are the reflection coefficients of the TM and the TE modes at the lower boundary of layer (l). They can be obtained recursively as

$$R^{\alpha}_{\cup l} = \frac{R^{\alpha}_{l(l-1)} + R^{\alpha}_{\cup(l-1)} e^{2ik_{(l-1)z}h_{l-1}}}{1 + R^{\alpha}_{l(l-1)} R^{\alpha}_{\cup(l-1)} e^{2ik_{(l-1)z}h_{l-1}}}, \qquad \alpha = (\mathrm{TE}, \mathrm{TM}) \tag{5a}$$

$$R^{\alpha}_{\cap l} = \frac{R^{\alpha}_{l(l+1)} + R^{\alpha}_{\cap(l+1)} e^{2ik_{(l+1)z}h_{l+1}}}{1 + R^{\alpha}_{l(l+1)} R^{\alpha}_{\cap(l+1)} e^{2ik_{(l+1)z}h_{l+1}}}, \qquad \alpha = (\mathrm{TE}, \mathrm{TM}) \tag{5b}$$

where $R^{\alpha}_{l(l-1)}$ and $R^{\alpha}_{l(l+1)}$ are the Fresnel reflection coefficients of the α mode across the interfaces at $z = -d_{l-1}$ and $z = -d_l$, respectively. The explicit forms are

$$R^{TE}_{l(l\pm1)} = \frac{k_{lz} - k_{(l\pm1)z}}{k_{lz} + k_{(l\pm1)z}} \qquad R^{TM}_{l(l\pm1)} = \frac{\epsilon_{l\pm1} k_{lz} - \epsilon_l k_{(l\pm1)z}}{\epsilon_{l\pm1} k_{lz} + \epsilon_l k_{(l\pm1)z}}. \tag{6}$$

Substituting the dyadic Green's function in (2) into (1), we obtain

$$\boldsymbol{E}(\boldsymbol{r}) + \frac{i\omega\mu_0 \Delta\sigma(\boldsymbol{r})}{k_l^2} \hat{z} E_z(\boldsymbol{r}) = -\frac{\omega\mu_0}{8\pi^2} \iiint_V dV' \iint_{-\infty}^{\infty} d\boldsymbol{k}_s e^{i\boldsymbol{k}_s \cdot (\boldsymbol{r}_s - \boldsymbol{r}'_s)} \Delta\sigma(\boldsymbol{r}') \cdot \bar{\bar{g}}_{ll}(\boldsymbol{k}_s, z, z') \cdot \boldsymbol{E}(\boldsymbol{r}') \tag{7}$$

where the source dyadic contribution has been collected to be the second term on the left-hand side. If the observation point is outside of the source region, this term vanishes automatically.

We assume that the pth eigenmode can be represented as $\boldsymbol{E}_p(\boldsymbol{\rho}) e^{i\eta y}$, where η is the propagation constant in the y direction, and $\boldsymbol{\rho} = \hat{x}x + \hat{z}z$. Equation (7) can thus be reduced to

$$\boldsymbol{E}_p(\boldsymbol{\rho}) + \frac{i\omega\mu_0 \Delta\sigma(\boldsymbol{\rho})}{k_l^2} \hat{z} E_{pz}(\boldsymbol{\rho}) = -\frac{\omega\mu_0}{4\pi} \iint_S d\boldsymbol{\rho}' \Delta\sigma(\boldsymbol{\rho}') \int_{-\infty}^{\infty} dk_x e^{ik_x(x-x')} \cdot \bar{\bar{g}}_{ll}(k_x, \eta, z, z') \cdot \boldsymbol{E}_p(\boldsymbol{\rho}') \tag{8}$$

where S is the cross section of the conductor strip, with $\Delta\sigma(\boldsymbol{\rho}) \neq 0$.

Consider two identical conductor strips embedded in layer (l) and located symmetrically with respect to $x = 0$. For such a structure, both an even and an odd mode exist. We define the even (odd) mode as a mode with E_z an even (odd) function, and H_z an odd (even) function of x. A magnetic (electric) plane can be inserted at $x = 0$ without affecting the field distributions.

The coupled integral equation can be rewritten as

$$\boldsymbol{E}_p(\boldsymbol{\rho}) + \frac{i\omega\mu_0 \Delta\sigma(\boldsymbol{\rho})}{k_l^2} \hat{z} E_{pz}(\boldsymbol{\rho}) = -\frac{\omega\mu_0}{4\pi} \iint_{S_1} d\boldsymbol{\rho}' \Delta\sigma(\boldsymbol{\rho}') \int_{-\infty}^{\infty} dk_x e^{ik_x(x-x')} \cdot \bar{\bar{g}}_{ll}(k_x, \eta, z, z') \cdot \boldsymbol{E}_p(\boldsymbol{\rho}') - \frac{\omega\mu_0}{4\pi} \iint_{S_2} d\boldsymbol{\rho}' \Delta\sigma(\boldsymbol{\rho}') \int_{-\infty}^{\infty} dk_x e^{ik_x(x-x')} \cdot \bar{\bar{g}}_{ll}(k_x, \eta, z, z') \cdot \boldsymbol{E}_p(\boldsymbol{\rho}'), \qquad \boldsymbol{\rho} \text{ on } S_1 \text{ or } S_2 \tag{9}$$

where S_1 and S_2 are the cross sections of the conductor strips. The source dyadic contribution has been collected as the second term on the left-hand side of (9). On the right-hand side of (9), the first (second) integral represents the contribution from the equivalent conduction and polarization current in the first (second) conductor strip.

In the next section, the Galerkin's method is used to solve the integral equations (8) and (9) for the dispersion relation $\eta(\omega)$.

III. Numerical Solution

Consider a conductor strip with a rectangular cross section of width w and thickness t. We first divide the width and thickness into N and M segments, respectively. The length of the nth segment in the x direction is w_n, and the length of the mth segment in the z direction is t_m, where $w_1 + \cdots + w_N = w$ and $t_1 + \cdots + t_M = t$. The center coordinate of the (n, m) cell, S_{nm}, is denoted by (x_n, z_m) with $1 \leq n \leq N$ and $1 \leq m \leq M$.

The electric field of the pth eigenmode on the cross section S can thus be represented by a set of pulse basis functions as

$$\boldsymbol{E}_p(\boldsymbol{\rho}) = \sum_{\beta = x,y,z} \sum_{n=1}^{N} \sum_{m=1}^{M} a^{\beta}_{nm} \hat{\beta} P_n(x - x_n) R_m(z - z_m) \tag{10}$$

where

$$P_n(x - x_n) = \begin{cases} 1, & x_n - w_n/2 \leq x \leq x_n + w_n/2 \\ 0, & \text{elsewhere} \end{cases} \tag{11a}$$

$$R_m(z - z_m) = \begin{cases} 1, & z_m - t_m/2 \leq z \leq z_m + t_m/2 \\ 0, & \text{elsewhere.} \end{cases} \tag{11b}$$

Substituting (10) and (11) into (8), we have

$$\sum_{\beta=x,y,z}\sum_{n=1}^{N}\sum_{m=1}^{M} a_{nm}^{\beta}\hat{\beta}P_n(x-x_n)R_m(z-z_m)\cdot\left[1+\frac{i\omega\mu_0\Delta\sigma_{nm}}{k_l^2}\delta_{\beta z}\right]$$
$$=-\frac{\omega\mu_0}{4\pi}\sum_{\beta=x,y,z}\sum_{n=1}^{N}\sum_{m=1}^{M} a_{nm}^{\beta}\Delta\sigma_{nm}\cdot\iint_{S_{nm}} d\boldsymbol{\rho}' P_n(x'-x_n)R_m(z'-z_m)$$
$$\times\int_{-\infty}^{\infty} dk_x e^{ik_x(x-x')}\bar{\bar{g}}_{ll}(k_x,\eta,z,z')\cdot\hat{\beta}, \qquad \boldsymbol{\rho}\text{ on } S \quad (12)$$

where $\delta_{\alpha\beta}$ is the Kronecker delta function, which is equal to one when $\alpha=\beta$, and is equal to zero when $\alpha\neq\beta$, and $\Delta\sigma_{nm}$ is the value of $\Delta\sigma(\boldsymbol{\rho})$ calculated at (x_n, z_m).

For conductor strips of arbitrary cross section, we can approximate the cross section by a mosaic of rectangles, and a field expression similar to (10) can be obtained.

Next, we choose the same set of basis functions as the testing functions, and apply the Galerkin's method to (12). Taking the inner product of $\hat{\alpha}P_r(x-x_r)R_q(z-z_q)$ with (12), we obtain

$$-\pi\omega\mu_0\sum_{\beta=x,y,z}\sum_{n=1}^{N}\sum_{m=1}^{M} a_{nm}^{\beta}\Delta\sigma_{nm}\cdot\int_{-\infty}^{\infty} dk_x e^{ik_x(x_r-x_n)}\tilde{P}_r(-k_x)\tilde{P}_n(k_x)\hat{g}_{\alpha\beta}^{qm}(k_x,\eta)$$
$$=A_{rq}\left[1+\frac{i\omega\mu_0\Delta\sigma_{rq}}{k_l^2}\delta_{\alpha z}\right]a_{rq}^{\alpha} \quad (13)$$

where $\alpha=x,y,z$; $1\leqslant r\leqslant N$ and $1\leqslant q\leqslant M$; A_{rq} is the area of S_{rq}; $\tilde{P}_n(k_x)$ is the Fourier transform of $P_n(x)$ with

$$\tilde{P}_n(k_x)=\frac{1}{2\pi}\int_{-w_n/2}^{w_n/2} dx\, e^{-ik_x x}P_n(x)=\frac{\sin(k_x w_n/2)}{\pi k_x} \quad (14)$$

and $\hat{g}_{\alpha\beta}^{qm}(k_x,\eta)$ is the $\alpha\beta$ component of the dyadic $\bar{\bar{g}}^{qm}(k_x,\eta)$ with

$$\bar{\bar{g}}^{qm}(k_x,\eta)=\int_{l_q} dz R_q(z-z_q)\cdot\int_{l_m} dz' R_m(z'-z_m)\bar{\bar{g}}_{ll}(k_x,\eta,z,z') \quad (15)$$

where l_q is the domain of $R_q(z-z_q)$. The integral in (15) can be done analytically because the variables z and z' of the dyadic Green's function appear only in the exponential terms as shown in (3).

By utilizing the symmetry properties of $\tilde{P}_n(k_x)$ and $\hat{g}_{\alpha\beta}^{qm}(k_x,\eta)$ with respect to k_x, (13) can further be reduced to

$$-2\pi\omega\mu_0\sum_{\beta=x,y,z}\sum_{n=1}^{N}\sum_{m=1}^{M} a_{nm}^{\beta}\Delta\sigma_{nm}\cdot\int_0^{\infty} dk_x\tilde{P}_r(k_x)\tilde{P}_n(k_x)W_{rq,nm}^{\alpha\beta}(k_x,\eta)$$
$$=\sum_{\beta=x,y,z}\sum_{n=1}^{N}\sum_{m=1}^{M}\delta_{\alpha\beta}\delta_{rn}\delta_{qm}A_{nm}\cdot\left[1+\frac{i\omega\mu_0\Delta\sigma_{nm}}{k_l^2}\delta_{\beta z}\right]a_{nm}^{\beta} \quad (16)$$

where

$$W_{rq,nm}^{\alpha\beta}(k_x,\eta)=\begin{cases}\cos k_x(x_r-x_n)\hat{g}_{\alpha\beta}^{qm}(k_x,\eta),\\ (\alpha,\beta)=(x,x),(y,y),(y,z),(z,y),(z,z)\\ i\sin k_x(x_r-x_n)\hat{g}_{\alpha\beta}^{qm}(k_x,\eta),\\ (\alpha,\beta)=(x,y),(x,z),(y,x),(z,x).\end{cases} \quad (17)$$

Equation (16) is a matrix equation of the form

$$\sum_{\beta=x,y,z}\sum_{n=1}^{N}\sum_{m=1}^{M} Z_{rq,nm}^{\alpha\beta}a_{nm}^{\beta}=0 \quad (18)$$

where $\alpha=x,y,z$; $1\leqslant r\leqslant N$ and $1\leqslant q\leqslant M$. The eigenvalue η can thus be obtained by setting the determinant of the Z matrix in (18) to zero, i.e.,

$$\det[Z(\omega,\eta)]=0. \quad (19)$$

Muller's method is then used to solve for the eigenvalue numerically.

To solve the integral equation (9) for two symmetrical conductor strips, we choose the same set of pulse basis functions as in (11) to represent the electric field on the cross section S_1 as

$$\boldsymbol{E}_p(\boldsymbol{\rho})=\sum_{\beta=x,y,z}\sum_{n=1}^{N}\sum_{m=1}^{M} a_{nm}^{\beta}\hat{\beta}P_n(x-x_n)R_m(z-z_m), \qquad \boldsymbol{\rho}\text{ on } S_1. \quad (20)$$

By symmetry, the electric field on the cross section S_2 can be represented as

$$\boldsymbol{E}_p(\boldsymbol{\rho})=\sum_{\beta=x,y,z}\sum_{n=1}^{N}\sum_{m=1}^{M} I_{\xi}^{\beta}a_{nm}^{\beta}\hat{\beta}P_n(x+x_n)R_m(z-z_m), \qquad \boldsymbol{\rho}\text{ on } S_2 \quad (21)$$

where the subscript ξ in I_{ξ}^{β} designates the even mode when $\xi=e$, and the odd mode when $\xi=o$. The definition of I_{ξ}^{β} is

$$I_{\xi}^{\beta}=\begin{cases}1, & (\xi,\beta)=(o,x),(e,y),(e,z)\\ -1, & (\xi,\beta)=(e,x),(o,y),(o,z).\end{cases} \quad (22)$$

Substituting (20) and (21) into (9) for ρ on S_1, we have

$$\sum_{\beta=x,y,z}\sum_{n=1}^{N}\sum_{m=1}^{M} a_{nm}^{\beta}\hat{\beta}P_n(x-x_n)R_m(z-z_m)\cdot\left[1+\frac{i\omega\mu_0\Delta\sigma_{nm}}{k_l^2}\delta_{\beta z}\right]$$
$$=-\frac{\omega\mu_0}{4\pi}\sum_{\beta=x,y,z}\sum_{n=1}^{N}\sum_{m=1}^{M} a_{nm}^{\beta}\Delta\sigma_{nm}\cdot\iint_{S_{nm}} d\rho'\left[P_n(x'-x_n)+I_{\xi}^{\beta}P_n(x'+x_n)\right]R_m(z'-z_m)\cdot\int_{-\infty}^{\infty} dk_x e^{ik_x(x-x')}\bar{\bar{g}}_{ll}(k_x,\eta,z,z')\cdot\hat{\beta},\qquad \rho \text{ on } S_1. \tag{23}$$

Owing to the symmetry of the structure, only the electric fields on S_1 need to be tested when applying the Galerkin's method. Taking the inner product of $\hat{\alpha}P_r(x-x_r)R_q(z-z_q)$ with (23) and utilizing the symmetry properties of the integrand with respect to k_x, we have

$$-2\pi\omega\mu_0\sum_{\beta=x,y,z}\sum_{n=1}^{N}\sum_{m=1}^{M} a_{nm}^{\beta}\Delta\sigma_{nm}\cdot\int_0^{\infty} dk_x\tilde{P}_r(k_x)\tilde{P}_n(k_x)W_{rq,nm}^{\alpha\beta(\xi)}(k_x,\eta)$$
$$=\sum_{\beta=x,y,z}\sum_{n=1}^{N}\sum_{m=1}^{M}\delta_{\alpha\beta}\delta_{rn}\delta_{qm}A_{nm}\cdot\left[1+\frac{i\omega\mu_0\Delta\sigma_{nm}}{k_l^2}\delta_{\beta z}\right]a_{nm}^{\beta} \tag{24}$$

where $\alpha=x,y,z$; $1\leqslant r\leqslant N$ and $1\leqslant q\leqslant M$; and

$$W_{rq,nm}^{\alpha\beta(\xi)}(k_x,\eta)=\begin{cases}\left[\cos k_x(x_r-x_n)+I_{\xi}^{\beta}\cos k_x(x_r+x_n)\right]\hat{g}_{\alpha\beta}^{qm}(k_x,\eta), & (\alpha,\beta)=(x,x),(y,y),(y,z),(z,y),(z,z)\\ i\left[\sin k_x(x_r-x_n)+I_{\xi}^{\beta}\sin k_x(x_r+x_n)\right]\hat{g}_{\alpha\beta}^{qm}(k_x,\eta), & (\alpha,\beta)=(x,y),(x,z),(y,x),(z,x).\end{cases} \tag{25}$$

Equation (24) is a matrix equation, and the eigenvalue η can be obtained by setting the determinant of the matrix to zero.

IV. Results and Discussions

In Fig. 2, we present the attenuation constant of a microstrip line of finite thickness embedded in a homogeneous medium. The results from a finite element method [13] are also presented for comparison. The deviation in the high-frequency range may be due to the truncation of structure in the finite element method.

Next, we present the propagation and attenuation constants of a stripline in Fig. 3. In this figure and the rest of the results, normal temperature is considered. Both copper (Cu) and molybdenum (Mo) are used to compare the effect of conductivity since these two materials are commonly used in

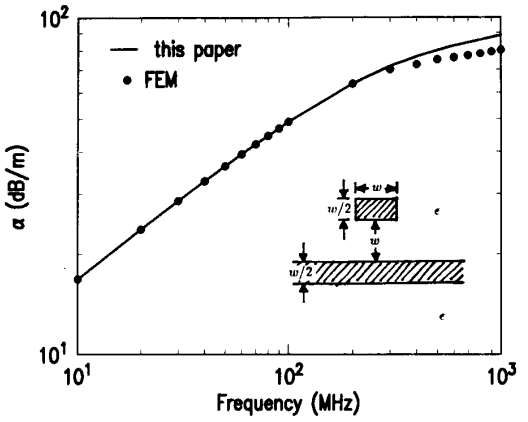

Fig. 2. Attenuation constant of a microstrip line of finite thickness embedded in a homogeneous medium, $w=2$ μm, $\epsilon=3.5\epsilon_0$, σ_{Cu} (77°) = 4.5×10^8 S/m.

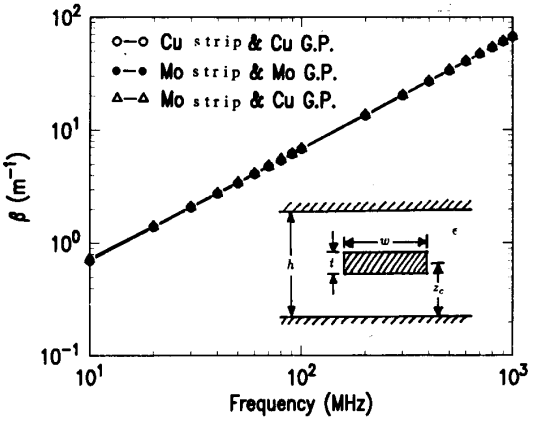

(a)

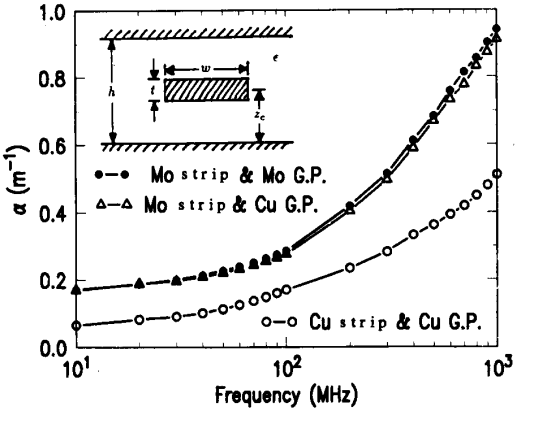

(b)

Fig. 3. Dispersion relation of a stripline: $w=100$ μm, $t=25$ μm, $h=600$ μm, $z_c=300$ μm, $\epsilon=10\epsilon_0$, $\sigma_{Cu}=5.92\times10^7$ S/m, $\sigma_{Mo}=1.92\times10^7$ S/m. (a) Propagation constant. (b) Attenuation constant.

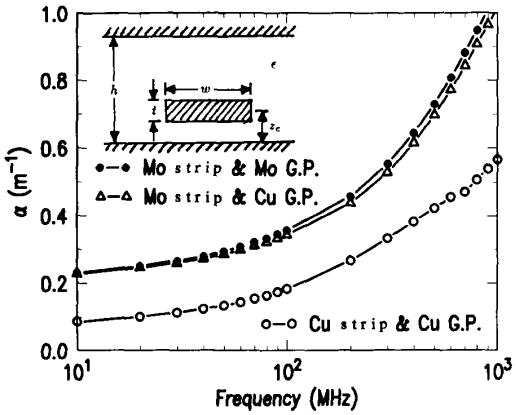

Fig. 4. Attenuation constant of a stripline: $w = 100\ \mu m$, $t = 25\ \mu m$, $h = 600\ \mu m$, $z_c = 200\ \mu m$, $\epsilon = 10\epsilon_0$, $\sigma_{Cu} = 5.92 \times 10^7$ S/m, $\sigma_{Mo} = 1.92 \times 10^7$ S/m.

the fabrication of interconnects in computer circuitries. For this structure, we divide the strip cross section into 14 by 6 small rectangles. The size of the rectangles closer to the strip surface is chosen to be smaller than the size of those farther away from the surface. Note that at the frequency of 100 MHz, the skin depths of Cu and Mo are about 6.54 μm and 11.49 μm, respectively. It is also found that although the magnitude of the transversal current is much smaller than that of the longitudinal (y) component, the results of the attenuation constant become unreasonable when the transversal currents are neglected. The computation was done by using an IBM 3090/600E mainframe computer, and the computation time is about a few seconds to obtain each curve.

In Fig. 3, it is observed that the propagation constant deviates slightly from that of the TEM mode. The attenuation constant approaches a constant as frequency is reduced, and becomes proportional to the square root of frequency at higher frequencies. The result for Mo strip and Mo ground plane is close to that for Mo strip and Cu ground plane. This implies that the conductor loss is mainly contributed by the strip.

In Fig. 4, we present the attenuation constant of a stripline where the strip is located closer to the lower ground plane. The attenuation constant is larger than that of the corresponding case in Fig. 3. Because the strip is closer to the lower ground plane, the field strength increases below the strip. Although the field strength is smaller between the strip and the upper ground plane than in Fig. 3, the overall conductor loss is increased. The propagation constant is close to the results in Fig. 3(a), and is not presented.

In Fig. 5, the cross section of the structure is scaled down by a factor of 10, and the frequency range is scaled up proportionally. It is observed that the propagation constant deviates more from that of the TEM mode than in Fig. 3. Meanwhile, the attenuation constant is much larger than that in Fig. 3.

In Fig. 6, we present the attenuation constant for a stripline with a square cross section of the same area as the cross section of the stripline in Fig. 3. The attenuation constants in both cases are roughly the same.

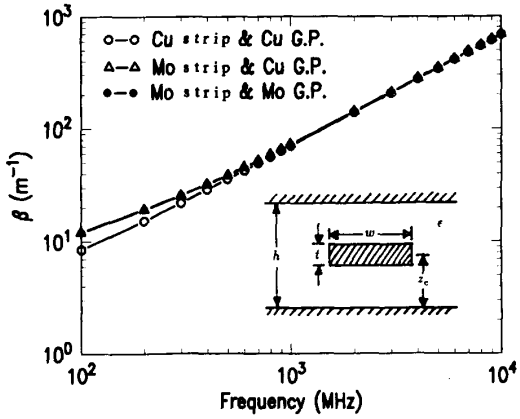

(a)

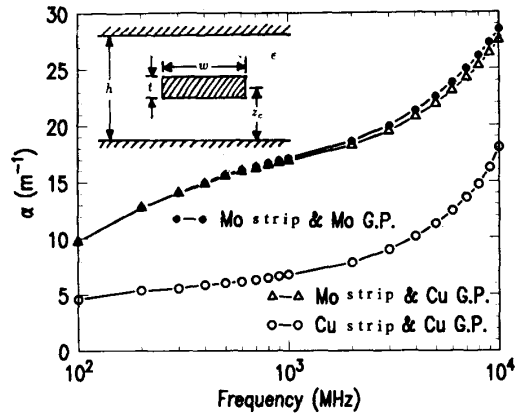

(b)

Fig. 5. Dispersion relation of a stripline: $w = 10\ \mu m$, $t = 2.5\ \mu m$, $h = 60\ \mu m$, $z_c = 30\ \mu m$, $\epsilon = 10\epsilon_0$, $\sigma_{Cu} = 5.92 \times 10^7$ S/m, $\sigma_{Mo} = 1.92 \times 10^7$ S/m. (a) Propagation constant. (b) Attenuation constant.

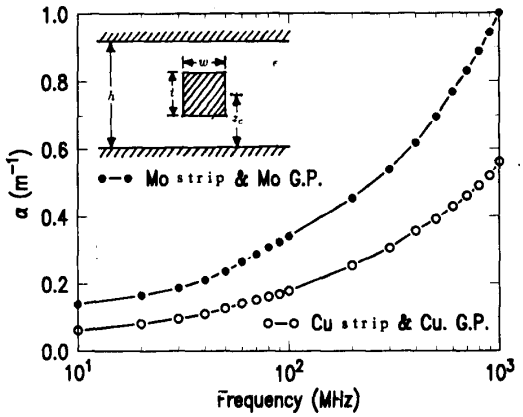

Fig. 6. Attenuation constant of a stripline: $w = 50\ \mu m$, $t = 50\ \mu m$, $h = 600\ \mu m$, $z_c = 300\ \mu m$, $\epsilon = 10\epsilon_0$, $\sigma_{Cu} = 5.92 \times 10^7$ S/m, $\sigma_{Mo} = 1.92 \times 10^7$ S/m.

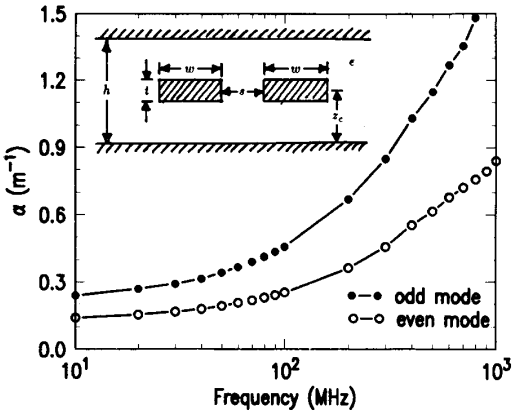

Fig. 7. Attenuation constant of two coupled striplines: $w = 100$ μm, $t = 25$ μm, $h = 600$ μm, $z_c = 300$ μm, $s = 100$ μm, $\epsilon = 10\epsilon_0$, $\sigma_{Mo} = 1.92 \times 10^7$ S/m.

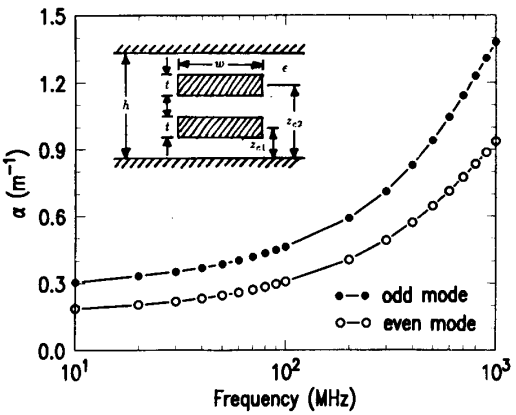

Fig. 9. Attenuation constant of two coupled striplines: $w = 100$ μm, $t = 25$ μm, $h = 600$ μm, $z_{c1} = 200$ μm, $z_{c2} = 400$ μm, $\epsilon = 10\epsilon_0$, $\sigma_{Mo} = 1.92 \times 10^7$ S/m.

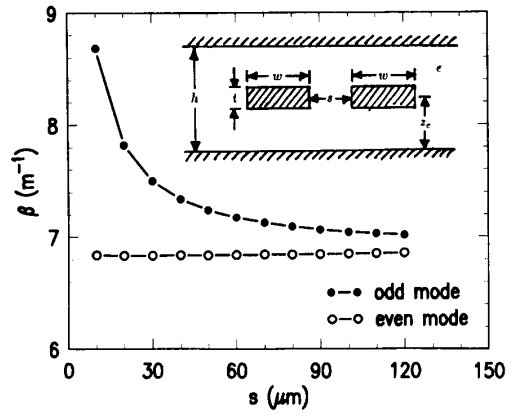

(a)

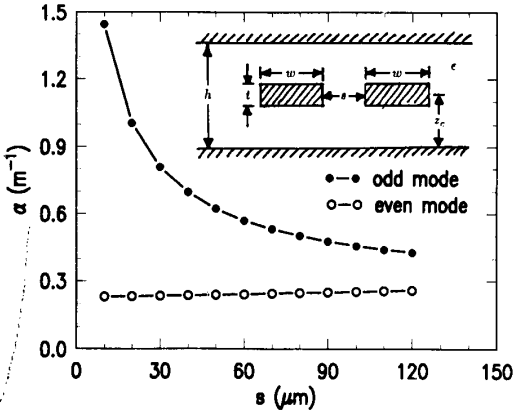

(b)

Fig. 8. Dispersion relation of two coupled striplines: $f = 100$ MHz, $w = 100$ μm, $t = 25$ μm, $h = 600$ μm, $z_c = 300$ μm, $\epsilon = 10\epsilon_0$, $\sigma_{Mo} = 1.92 \times 10^7$ S/m. (a) Propagation constant. (b) Attenuation constant.

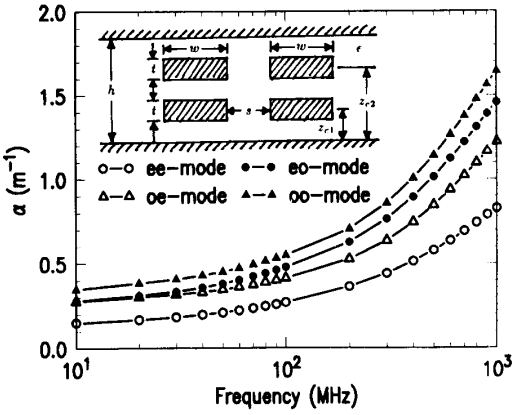

Fig. 10. Attenuation constant of four coupled striplines: $w = 100$ μm, $t = 25$ μm, $h = 600$ μm, $z_{c1} = 200$ μm, $z_{c2} = 400$ μm, $s = 100$ μm, $\epsilon = 10\epsilon_0$, $\sigma_{Mo} = 1.92 \times 10^7$ S/m.

In Fig. 7, the attenuation constants of two coupled striplines are presented. The separation s between the two strips is defined as the shortest distance between them. The attenuation constant of the odd mode is larger than that of the even mode owing to the difference of field distributions.

In Fig. 8, we present the propagation and attenuation constants of both modes as a function of the separation between the two strips. It is observed that the results for the even mode are less sensitive to the separation than the odd mode. This is because the field distribution of the odd mode changes more drastically than that of the even mode as the separation is changed.

The attenuation constants of two coupled striplines in an up–down arrangement are presented in Fig. 9. Again, the attenuation constant of the odd mode is larger than that of the even mode. The propagation constants for both modes are very close to that in Fig. 3(a) and hence are not presented.

Next, we present the attenuation constant for a symmetrical structure consisting of four strips as shown in the inset of Fig. 10. There are four fundamental modes, indicated by *ee*,

Even/Odd Parity of Field Components			
mode	E_x	E_y	E_z
ee	− + − +	+ + + +	+ + − −
eo	+ + + +	− + − +	− + + −
oe	− + + −	+ + − −	+ + + +
oo	+ + − −	− + + −	− + − +

Fig. 11. The even/odd parity of the electric field components, the first (second) symbol is with respect to the horizontal (vertical) center line: + even symmetry; − odd symmetry.

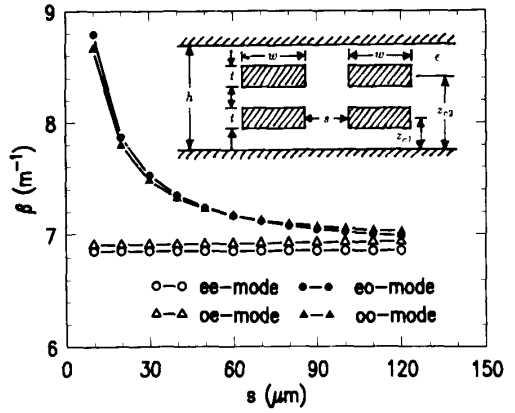

(a)

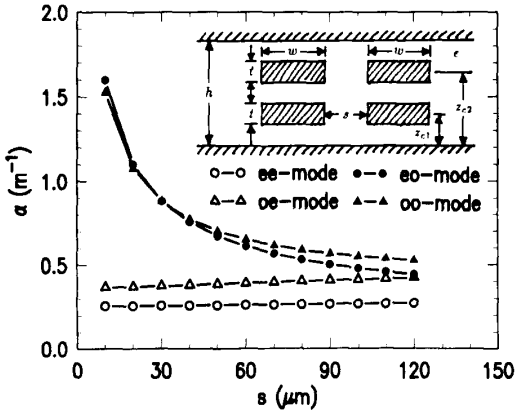

(b)

Fig. 12. Dispersion relation of four coupled striplines: $f = 100$ MHz, $w = 100$ μm, $t = 25$ μm, $h = 600$ μm, $z_{c1} = 200$ μm, $z_{c2} = 400$ μm, $\epsilon = 10\epsilon_0$, $\sigma_{Mo} = 1.92 \times 10^7$ S/m. (a) Propagation constant. (b) Attenuation constant.

eo, *oe*, and *oo*, respectively. The first symbol indicates the symmetry with respect to the horizontal center line, and the second symbol indicates the symmetry with respect to the vertical center line. The even/odd parity of all the field components is shown in Fig. 11, where the + (−) sign represents an even (odd) symmetry with respect to the center line.

As shown in Fig. 10, the attenuation constant of the *ee* mode is the smallest, and that of the *oo* mode is the largest. This again is due to the field distributions of different modes. The propagation constants of these four modes are all close to that of the TEM mode for a single stripline.

In Fig. 12, we present the results of four different modes as a function of horizontal separation. It is observed that the *ee* and *oe* modes are less sensitive to the horizontal separation because these two modes have an even symmetry with respect to the vertical center line.

V. Conclusions

An integral equation formulation utilizing the dyadic Green's function is proposed to calculate the conductor loss in a rigorous way. Galerkin's method is used to solve the integral equation for the dispersion relation where the conductor loss is incorporated in the attenuation constant. The attenuation properties for different stripline structures used in the packages of high-performance computer circuitries are presented.

References

[1] R. F. Harrington and C. Wei, "Losses on multiconductor transmission lines in multilayered dielectric media," *IEEE Trans. Microwave Theory Tech.*, vol. MTT-32, pp. 705–710, July 1984.

[2] B. E. Spielman, "Dissipation loss effects in isolated and coupled transmission lines," *IEEE Trans. Microwave Theory Tech.*, vol. MTT-25, pp. 648–656, Aug. 1977.

[3] Z. Pantic and R. Mittra, "Quasi-TEM analysis of microwave transmission lines by the finite-element method," *IEEE Trans. Microwave Theory Tech.*, vol. MTT-34, pp. 1096–1103, Nov. 1986.

[4] D. M. Syahkal and J. B. Davies, "Accurate solution of microstrip and coplanar structures for dispersion and for dielectric and conductor losses," *IEEE Trans. Microwave Theory Tech.*, vol. MTT-27, pp. 694–699, July 1979.

[5] T. E. Van Deventer, P. B. Katehi, and A. C. Cangellaris, "An integral equation method for the evaluation of conductor and dielectric losses in high-frequency interconnects," *IEEE Trans. Microwave Theory Tech.*, vol. 37, pp. 1964–1972, Dec. 1989.

[6] J. M. Pond, C. M. Krowne, and W. L. Carter, "On the application of complex resistive boundary conditions to model transmission lines consisting of very thin superconductors," *IEEE Trans. Microwave Theory Tech.*, vol. 37, pp. 181–190, Jan. 1989.

[7] R. A. Pucel, D. J. Masse, and C. P. Hartwig, "Losses in microstrip," *IEEE Trans. Microwave Theory Tech.*, vol. MTT-16, pp. 342–350, June 1968.

[8] R. A. Pucel, D. J. Masse, and C. P. Hartwig, Correction to "Losses in microstrip," *IEEE Trans. Microwave Theory Tech.*, vol. MTT-16, p. 1064, Dec. 1968.

[9] H. A. Wheeler, "Formulas for the skin effect," *Proc. IRE*, vol. 30, pp. 412–424, Sept. 1942.

[10] A. Konrad, "Integrodifferential finite element formulation of two-dimensional steady-state skin effect problems," *IEEE Trans. Magn.*, vol. MAG-18, pp. 284–292, Jan. 1982.

[11] G. I. Costache, "Finite element method applied to skin-effect problems in strip transmission lines," *IEEE Trans. Microwave Theory Tech.*, vol. MTT-35, pp. 1009–1013, Nov. 1987.

[12] P. Waldow and I. Wolff, "The skin-effect at high frequencies," *IEEE Trans. Microwave Theory Tech.*, vol. MTT-33, pp. 1076–1082, Oct. 1985.
[13] U. S. Ghoshal and L. N. Smith, "Skin effects in narrow copper microstrip at 77 K," *IEEE Trans. Microwave Theory Tech.*, vol. 36, pp. 1788–1795, Dec. 1988.
[14] R. L. Kautz, "Miniaturization of normal-state and superconducting striplines," *J. Res. Nat. Bur. Stand.*, vol. 84, no. 3, pp. 247–259, May 1979.
[15] H. Y. Lee and T. Itoh, "Phenomenological loss equivalence method for planar quasi-TEM transmission lines with a thin normal conductor or superconductor," *IEEE Trans. Microwave Theory Tech.*, vol. 37, pp. 1904–1909, Dec. 1989.
[16] M. J. Tsuk and J. A. Kong, "The frequency-dependent resistance of conductors with arbitrary cross-sections," in *Proc. Progress in Electromag. Res. Symp.*, July 1989, pp. 251–252.
[17] A. R. Djordjevic, T. K. Sarkar, and S. M. Rao, "Analysis of finite conductivity cylindrical conductors excited by axially-independent TM electromagnetic field," *IEEE Trans. Microwave Theory Tech.*, vol. MTT-33, pp. 960–966, Oct. 1985.
[18] C. W. Ho, D. A. Chance, C. H. Bajorek, and R. E. Acosta, "The thin-film module as a high-performance semiconductor package," *IBM J. Res. Develop.*, vol. 26, no. 3, pp. 286–296, May 1982.
[19] R. J. Jensen, J. P. Cummings, and H. Vora, "Copper/polyimide materials system for high performance packaging," *IEEE Trans. Components, Hybrids, Manuf. Technol.*, vol. CHMT-7, pp. 384–393, Dec. 1984.
[20] O. K. Kwon, B. W. Langley, R. F. W. Pease, and M. R. Beasley, "Superconductors as very high-speed system-level interconnects," *IEEE Electron Device Lett.*, vol. EDL-8, pp. 582–585, Dec. 1987.
[21] J. F. Kiang, S. M. Ali, and J. A. Kong, "Propagation properties of striplines periodically loaded with crossing strips," *IEEE Trans. Microwave Theory Tech.*, vol. 37, pp. 776–786, Apr. 1989.
[22] J. A. Kong, *Electromagnetic Wave Theory*. New York: Wiley, 1986.
[23] S. M. Ali, T. M. Habashy, and J. A. Kong, "Dyadic Green's functions for multilayered uniaxially anisotropic media," submitted to *J. Electromag. Waves Appl.*

✠

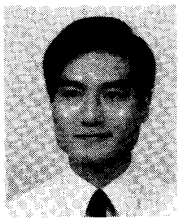

Jean-Fu Kiang (S'87–M'89) was born in Taipei, Taiwan, Republic of China, on February 2, 1957. He obtained the B.S.E.E. and M.S.E.E. degrees from the Department of Electrical Engineering, National Taiwan University, Taiwan, in 1979 and 1981, respectively. He came to the Department of Electrical Engineering and Computer Sciences, Massachusetts Institute of Technology, Cambridge, in September 1983 as a research and teaching assistant and obtained the M.S.E.E. and Ph.D. degrees there in 1985 and March 1989, respectively.

During the summers of 1985 and 1986, he worked at the Schlumberger-Doll Research Laboratory, Ridgefield, CT. From March 1989 to May 1990, he was with the IBM Thomas J. Watson Research Center, Yorktown Heights, NY. He joined Bell Communications Research, Red Bank, NJ, in June 1990.